Vegetation Sensing Using GPS Interferometric Reflectometry: Experimental Results With a Horizontally Polarized Antenna

Qiang Chen, Daehee Won, Dennis M. Akos, and Eric E. Small

***Abstract*—Measurement of vegetation state is required both for modeling and for satellite data validation. GPS Interferometric Reflectometry (GPS-IR) is a passive microwave remote sensing technique that has been applied to several applications, such as sensing soil moisture, snow depth, ocean roughness and wind speed, and vegetation growth. Previous studies proposed that geodetic GPS data could be used to measure vegetation biophysical parameters, for example, vegetation height and vegetation water content (VWC). However, the measurement range and accuracy are limited because the geodetic GPS antenna is designed to suppress reflections. In this paper, the antenna design for vegetation sensing via GPS-IR is discussed. Then, a customized dipole antenna is developed specifically for vegetation sensing. A field experiment is conducted at Boulder, CO, USA to evaluate the performance of the proposed antenna. The GPS metric, which is the normalized signal-to-noise ratio (SNR) amplitude A_{norm}, shows a linear relationship with *in situ* measurements of VWC over a range of 0—6 kg/m^2, which is much greater than the range from the geodetic data (0—1.0 kg/m^2). The sensitivity of A_{norm} to VWC change is -0.11 (W/W)/(kg/m^2), and the average measurement error of VWC is $\sim$12.4%. Thus, the horizontally polarized antenna is suitable for vegetation monitoring in most environments, including agricultural settings. The effects of soil moisture on GPS SNR amplitude are also documented, but these are minor compared to the decrease in amplitude resulting from vegetation growth.**

***Index Terms*—Global positioning system (GPS), reflectometry, remote sensing.**

I. Introduction

THE amount of water stored in vegetation is an important biophysical parameter for both climate and hydrological studies, and the measurement of vegetation water content (VWC) has been an important application of the remote sensing techniques, including optical and active/passive microwave bands [1], [2]. Among the passive microwave techniques, GPS Interferometric Reflectometry (GPS-IR) has proven its utility in various earth environmental sensing applications, including the measurements of snow depth [3]–[8], near-surface soil moisture [9]–[14], costal sea level [15]–[18], and vegetation biophysical parameters [12], [19]–[23]. The GPS-IR technique utilizes the interference pattern of the observed signal-to-noise ratio (SNR) created by the direct and ground reflected signals for environmental parameters retrieval (see Fig. 1).

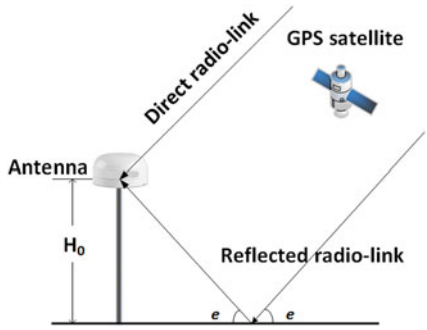

Fig. 1. Principle of GPS-IR. e is the elevation angle of the satellite with respect to the horizon, H_0 is the apparent height of the GPS antenna above the reflecting surface. GPS-IR is essentially a bistatic radar system. The GPS satellites serve as the radar transmitters and the ground-based GPS antennas/receivers serve as the radar receivers. There are two radio links: the direct and the reflected radio links. The reflected signal contains the information about the surface reflector. The primary observable used in GPS-IR is the SNR), which is a standard output for most GPS receivers. The SNR data exhibit an interference pattern created by the direct and reflected GPS signals.

One approach of the GPS-IR technique is utilizing the geodetic-quality GPS antennas and receivers that are mainly deployed for tectonic and surveying applications. The widely distributed geodetic GPS networks, e.g., Continuously Operating Reference Station (CORS, http://geodesy.noaa.gov/CORS) and the EarthScope Plate Boundary Observatory (PBO, http://pbo.unavco.org), provide wide spatial coverage, and have zero additional hardware cost for this capability expansion [24]. However, the geodetic GPS antennas are designed to suppress the ground reflected signal (known as multipath in GPS precise positioning) that contains the desired information about the earth's surface. Fig. 2(a) depicts the gain pattern of a typical geodetic GPS antenna. Generally, the right-handed circularly polarized (RHCP) gain is several orders of magnitude larger than the left-handed circularly polarized (LHCP) gain at high elevation angles, which aims to suppress the reflected GPS signal. That is because the direct or line-of-sight GPS signal is RHCP, and thus a portion of the reflected signal is cross polarized to be LHCP. Moreover, the RHCP gain is optimized for the zenith direction and minimized for the bottom hemisphere, which is another design feature to suppress the ground reflected signal. Fig. 2(b) shows some representative geodetic SNR time series

Manuscript received September 12, 2015; revised January 8, 2016 and March 7, 2016; accepted April 25, 2016. Date of publication May 26, 2016; date of current version October 14, 2016.

Q. Chen, D. Won, and D. M. Akos are with the Department of Aerospace Engineering Sciences, University of Colorado, Boulder, CO 80309-0429 USA (e-mail: qiang.chen@colorado.edu; daehee.won@colorado.edu; dma@colorado.edu).

E. E. Small is with the Department of Geological Sciences, University of Colorado, Boulder, CO 80309-0399 USA (e-mail: eric.small@colorado.edu).

Color versions of one or more of the figures in this paper are available online at http://ieeexplore.ieee.org.

Digital Object Identifier 10.1109/JSTARS.2016.2565687

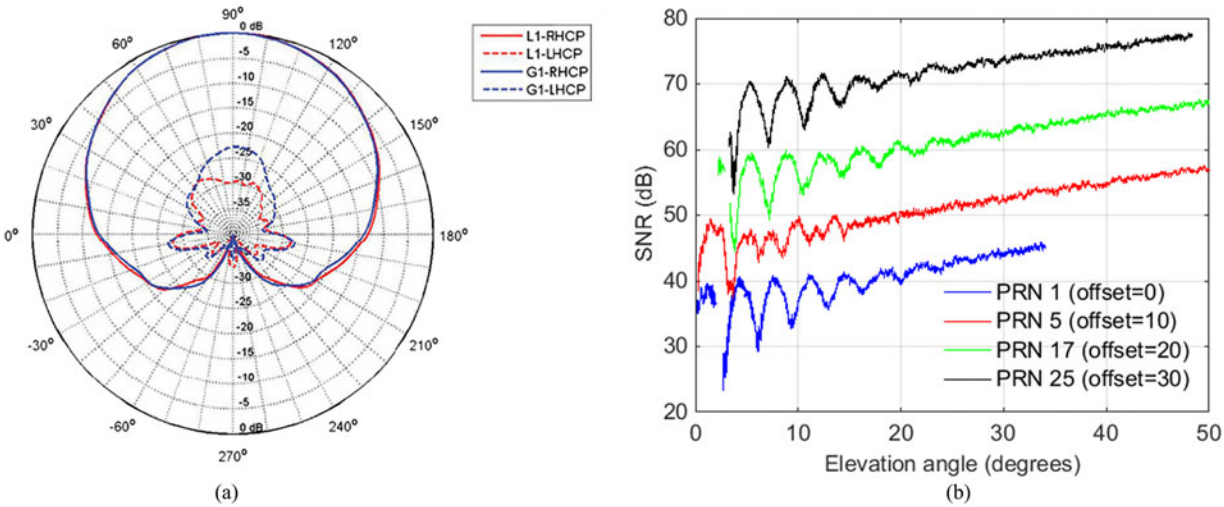

Fig. 2. (a) Novatel GPS-702-GG pinwheel antenna gain pattern (http://www.navtechgps.com/assets/). The solid red and blue curves are the RHCP gains of GPS L1 (1575.42 MHz) and GLONASS G1 (1602 MHz). The dashed red and blue curves are the LHCP gains of L1 and G1. (b) Some representative geodetic SNR time series with an antenna ∼2 m above the ground [25]. The four SNR time series (PRN 1, 5, 17, 25) are offset for clarity.

[25]. All four SNR time series show a rising trend as the elevation angle increases, as a result of the zenith optimization of the geodetic antenna's gain pattern. The interference pattern is more distinct at low elevation angles and diminishes at high-elevation angles. A reason is that the RHCP gains are comparable for the direct and ground reflected signals at low-elevation angles but are vastly different at high-elevation angles. For example, the RHCP gain difference presented in Fig. 2(a) is ∼5 dB for direct and reflected signals when the elevation angle is 10°. In addition, the natural surface produces more RHCP reflections at low-elevation angles. The limitations of the geodetic GPS antenna are discussed in [11] in detail.

To overcome the limitations of the geodetic GPS antenna, researchers have tried to utilize specifically designed antennas based on the requirements of the corresponding applications. In [12], [26], and [27], an instrument called Soil Moisture Interference-pattern GNSS Observations at L-band (SMIGOL) is proposed to retrieve land geophysical parameters (surface topography, vegetation height, and soil moisture). The key design of SMIGOL is utilizing a vertically polarized (V-pol) patch antenna to exclusively receive the V-pol components from the direct and reflected signals. Vertical polarization has an important feature known as the Brewster's angle: the angle at which the incident electromagnetic wave completely penetrates the bottom media and is not reflected. For bare soil, the V-pol SNR shows a notch in the interference pattern and, more importantly, the notch position is related to the permittivity of the soil, and thus determined by the soil moisture. If the notch is detected then it can be used for soil moisture retrieval. This technique is then extended to a dual-polarization configuration to add the horizontal polarization for more accurate soil moisture retrievals [13], [14]. For vegetation-covered soil, the interference pattern of the V-pol SNR has more than one notch and their number/positions are only determined by the vegetation height. Three field experiments were carried out during the year 2008–2010 in Spain with three types of crops: wheat, barley, and maize. The retrieved vegetation heights and *in situ* measurements match with high R^2 values ($R^2 > 0.79$). However, this study only presents the vegetation height retrievals and does not mention the possibility of retrieving other vegetation biophysical parameters (e.g., VWC).

Rather than utilizing the V-pol signal, other studies use the amplitude of the interference pattern of the geodetic SNR for vegetation parameter retrieval. In this paper, SNR amplitude refers to the amplitude of the interference pattern of the SNR time series unless otherwise specified. In [22], the agreement between the normalized SNR amplitude (normalized to bare soil SNR) and VWC is evaluated using field data for four vegetation types: shrub, short-grass, wheat, and alfalfa. It is concluded that the VWC shows a quasi-linear relationship with the normalized SNR amplitude. However, the linear relationship breaks down if the VWC exceeds 1.0 kg/m^2. In a companion paper [23], an electrodynamic model is proposed to simulate the response of geodetic SNR data to the changes in both soil moisture and vegetation. The model is validated against sampled field data, and predicts that the SNR amplitude is linearly related to the VWC provided that VWC is below a threshold of 1.5 kg/m^2. This measurement limitation deems geodetic SNR data inappropriate for vegetation sensing in many environments, including most agricultural settings. In this study, we follow up the work in [22] and [23] and propose a customized dipole GPS L1 antenna specifically designed for vegetation sensing. The SNR amplitude is used as the GPS metric. The performance of the proposed antenna is evaluated through an experimental campaign carried out on a farm planted with alfalfa in Boulder, CO, USA. At the same time, *in situ* vegetation and soil moisture are sampled to validate the GPS data. The effect of soil moisture on the GPS metric is evaluated in addition to retrieval of VWC.

This paper is organized as follows. Section II reviews the principle of the GPS-IR remote sensing technique. The formulation of the GPS-IR metrics is discussed. Section III presents the proposed antenna and introduces its characteristics. Section IV introduces the experimental setup, *in situ* data collection, and

GPS data analysis. The experimental results are summarized in Section V. The relationships between the GPS metric and vegetation measurements are described. In addition, the effect of soil moisture change on the GPS metric is discussed.

II. GPS-IR Metric Model

In this section, we briefly review the model of GPS metrics used in GPS-IR, especially the SNR amplitude that is the metric used in the vegetation sensing. The SNR data from a GPS receiver are formulated as [11], [28]

$$\mathrm{SNR} = (P_d + P_r + 2\sqrt{P_d P_r}\cos(2\pi f_m \sin e + \phi))/P_n \quad (1)$$

where P_d is the power of the direct signal, P_r is the power of the reflected signal, e is the elevation angle of the GPS satellite, f_m is the frequency, ϕ is the initial interference phase, and P_n is the noise power. For the geometry-driven applications (snow depth, coastal sea level), the frequency f_m is related to the antenna height with respect to the reflector H by

$$H = \frac{\lambda}{2} f_m \quad (2)$$

where λ is the wave length ($\lambda_{L1} = 19.0\,\mathrm{cm}$). When the satellite is rising or setting, the observed SNR shows an interference pattern with peaks and valleys when the direct and ground reflected signals are in phase or out of phase. The frequency f_m (and thus the antenna height H) can be estimated using the Lomb-Scargle Periodogram (LSP) that is similar to Discrete Time Fourier Transform but does not require evenly sampling. Some other frequency retrieval algorithms are discussed in [18]. The frequency derived antenna height is often referred to as effective reflector height H_{eff} [22], [23] and it is not always equal to the geometrical antenna height—for a geodetic antenna, the nonnegligible LHCP gain and the layering effect of soil medium are the primary reasons for this discrepancy [11].

If the receiving antenna is working on a single dominant polarization (this assumption does not hold for the geodetic antenna at low-elevation angles), the initial interference phase ϕ is formulated as

$$\phi = \phi_r + \phi_a \quad (3)$$

where

$$\phi_r = \arg(R_x) \quad (4)$$

is the phase of the complex Fresnel reflection coefficient R_x. Here, x indicates the polarization. The characteristics of ϕ_r for different polarizations and medium are discussed in detail in Section III. The term

$$\phi_a = \Theta(-e) - \Theta(e) \quad (5)$$

reflects the different phase response of the antenna at different elevation angles, where $\Theta(e)$ is the phase pattern of the receiving antenna at elevation angle e. The initial interference phase ϕ is not constant but changes much slower than the geometry-driven phase change because of the movement of the GPS satellite.

In vegetation sensing, the amplitude of the interference pattern $A \propto 2\sqrt{P_d P_r}$ is more sensitive to the change of VWC and, thus, is used for VWC measurement. The limitations of using effective height H and the interference phase ϕ as the GPS metric are discussed in [22] and [23]. The amplitude A is formulated as

$$A = 2|R_x S|\sqrt{G(e)G(-e)}P_{d,\mathrm{iso}}/P_n \quad (6)$$

where $P_{d,\mathrm{iso}}$ is the received power of the direct GPS signal by an isotropic antenna (about - 160 dBW above the earth surface), $G(e)$ is the gain pattern of the receiving antenna at e. For a surface reflector, S is the attenuation factor caused by the roughness of reflector and is computed by

$$S^2 = \exp(-4k^2 s^2 \sin^2 e) \quad (7)$$

where $k = 2\pi/\lambda$ is the wave number in free space; s is the standard deviation of ground surface height. In the various stages of the vegetation growth cycle, the amplitude A would change primarily with the reflection coefficient $|R_x|$ as a result of the vegetation state (vegetation height and VWC) changes. The response of $|R_x|$ to the change of vegetation state is discussed in Section III.

III. Antenna Design

In this section, we first present the Fresnel reflection coefficients of four polarizations: horizontal, vertical, right-handed circular (RHC) to RHC, and RHC to left-handed circular (LHC) for various vegetation states. The horizontal polarization is selected for vegetation sensing. At last, we introduce a customized dipole antenna to be used in the experiment, including its polarization and gain pattern.

A. Polarization Selection

For simplicity, the vegetation canopy is regarded as an attenuation layer that is proportional to VWC [29]. A more precise model to evaluate the effect of vegetation canopy can be found in [23] and is used in the following simulations. In Fig. 3, the simulated Fresnel reflection coefficients for vertical, horizontal, RHC to RHC, and RHC to LHC polarizations are presented. For each polarization, the reflection coefficients are calculated with four cases: dry bare soil, wet bare soil, 30-cm vegetation on top of the wet soil, and 60-cm vegetation on top of the wet soil. The permittivities of dry soil, wet soil, and vegetation canopy are $4 + 0.5\mathrm{j}$, $12 + 1.5\mathrm{j}$, and $1.06 + 0.013\mathrm{j}$, respectively, [11], [23].

For the bare soil cases, the magnitude of the horizontal Fresnel reflection coefficient $|R_h|$ is affected by soil moisture—$|R_h|$ increases as soil moisture gets larger [see Fig. 3(a)]. The overall horizontal reflection coefficient magnitude $|R_h|$ decreases as the vegetation grows. For vegetation covered soil, $|R_h|$ does not exhibit a monotonic change but has small variations. These variations are caused by the layering effect—the two leading outgoing reflections, which occur at the air-vegetation and the vegetation-soil interfaces, respectively, add up coherently in the air half-space. The reflection magnitude varies because the phase shift between the two reflections changes when satellite is rising or setting. The behaviors of $|R_{\mathrm{rr}}|$ are similar to $|R_h|$ [see Fig. 3(c)], but is minimally impacted by the soil moisture for bare soil cases. $|R_{\mathrm{rr}}|$is also affected by vegetation growth, but the

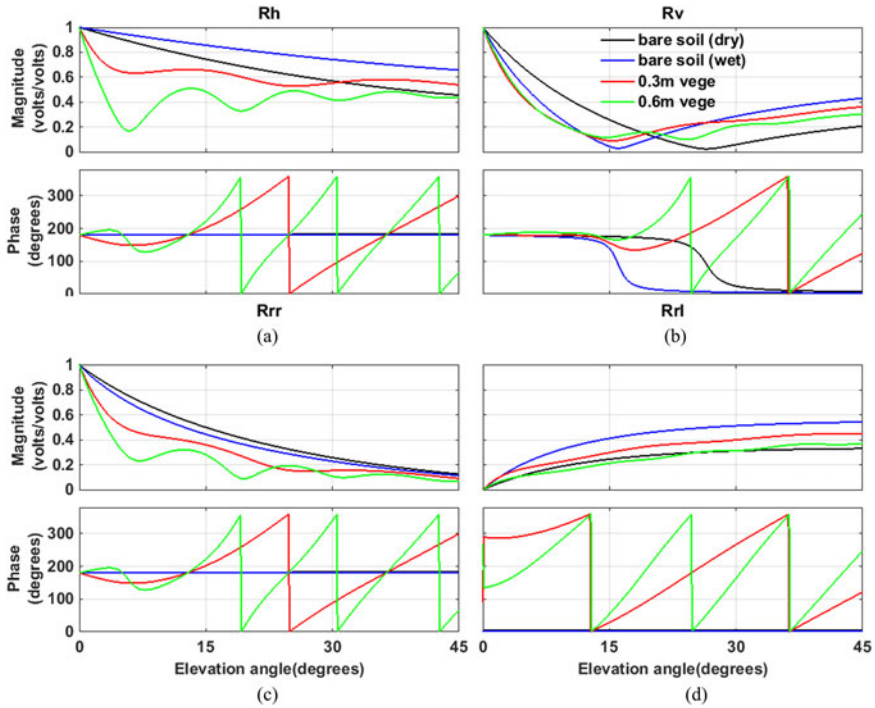

Fig. 3. Fresnel reflection coefficients of (a) horizontal, (b) vertical, (c) RHC to RHC, (d) RHC to LHC polarizations. For each polarization, the reflection coefficients are calculated for four cases: dry bare soil, wet bare soil, 30-cm vegetation on top of wet soil, and 60-cm vegetation on top of wet soil.

change of $|R_{\rm rr}|$ is not as distinct as $|R_h|$—the curves of $|R_{\rm rr}|$ for 0.3- and 0.6-m vegetation almost coincide. The drawback of this characteristic is that the GPS metric (SNR amplitude) gets saturated as the vegetation grows, as demonstrated in [22] and [23].

The behavior of $|R_v|$ [see Fig. 3(b)] matches the results presented in [12], [26] and [27]. For bare soil cases, there is only one minimum, corresponding to the Brewster's angle, in the curve of $|R_v|$. The position of the Brewster's angle is related to soil moisture and, thus, is used for soil moisture retrieval. As the vegetation grows, there are more minima and their number/positions change with the vegetation canopy height. However, it could be potentially difficult to detect the minima from the observed SNR because $|R_v|$ is relatively small (thus $|A|$ is also small) at the minima. The experimental data presented in Section IV demonstrate this difficulty.

$|R_{\rm rl}|$ is also affected by soil moisture for bare soil cases, as shown in Fig. 3(d). $|R_{\rm rl}|$ shows a monotonic change as the vegetation grows. However, $|R_{\rm rl}|$ is smaller than $|R_h|$ for the same vegetation state. For example, $|R_{\rm rl}|$ is only about 0.5 when elevation angle is around 20° for the bare soil case, and $|R_h|$ is around 0.8 at the same elevation angles. Again, a small reflection coefficient magnitude (and, thus, a small $|A|$) increases the possibility that the interference pattern is blurred.

B. Customized Antenna

In [25], a customized dipole antenna is proposed and evaluated in a snow depth sensing experiment carried out at Table Mountain plateau, Colorado during February 2012. The photograph of the antenna, the simulation model, and its simulated

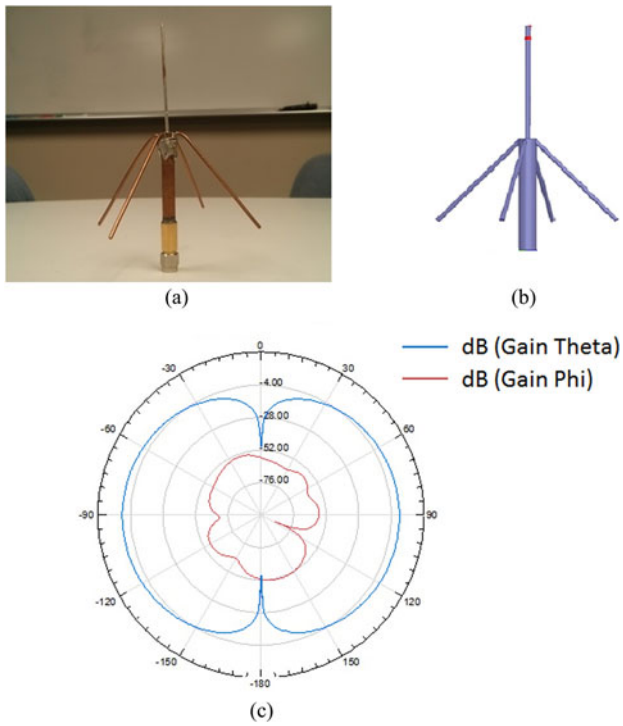

Fig. 4. (a) Antenna used in the vegetation experiment, first proposed in [25]. The working frequency is decided by the length of the top pin, and the input impedance can be adjusted to 50 Ω by bending the four legs; (b) simulation model of the proposed antenna in HFSS; and (c) simulated gain pattern of the proposed antenna. The gain at ϕ direction is negligible compared to the gain at θ direction, which means the dipole antenna is vertically polarized. If the antenna is tipped, it is horizontally polarized at $\theta = 90°$. Please note that there are two nulls in the direction of the antenna pointing and its opposite direction, which means there will be little signal received in these two directions.

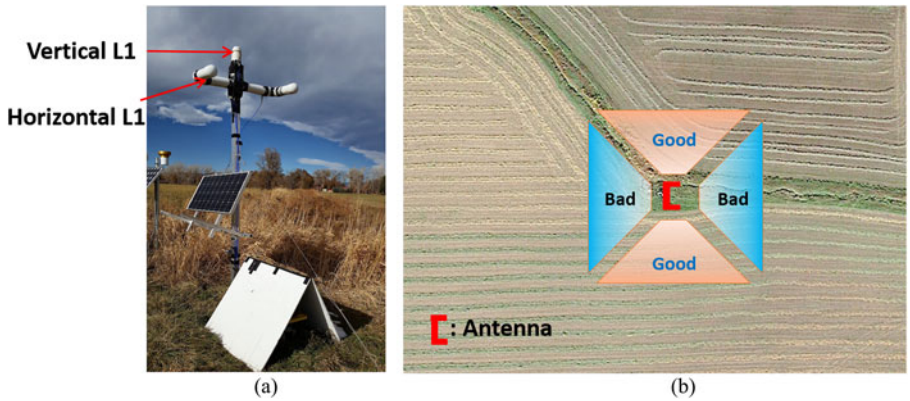

Fig. 5. (a) Photograph of the vegetation sensor. Two GPS antennas (H-pol L1 and V-pol L1) are utilized. The horizontal antenna is approximately 3 m above the ground. (b) The horizontal antennas are east oriented, so the sensing region is the south area (few ground tracks to the north direction).

gain pattern are presented in Fig. 4. The dipole antenna can be utilized in both vertical and horizontal polarization configurations. In the vegetation experiment described later, two dipole antennas, one vertically polarized and one horizontally polarized, are employed to output the H-pol and V-pol SNR. We conclude that the H-pol antenna is more useful to retrieve VWC over the range that exists in agricultural settings. Results from V-pol antenna are included to validate the simulation results presented earlier, and to show that the V-pol VWC measurement range is limited compared to that from the H-pol antenna.

IV. Experimental Setup and Data Collection

In this section, we describe an experimental campaign using the proposed dipole antenna. The experiment was carried out from May to August 2014 at an alfalfa farm in Boulder, CO, USA. First, we describe the experimental setup and then the methods of data collection for both *in situ* measurements and GPS data.

A. Experiment Setup

The assembled vegetation sensor is shown in Fig. 5(a). A 100-W solar panel is employed to provide power to the whole system. A mobile cellular radio is used to provide remote connectivity. This vegetation sensor employs two GPS antennas: a vertically polarized L1 and a horizontally polarized L1. Two low cost GlobalTop GPS L1 receivers are used to collect the SNR data from the H-pol and V-pol L1 antennas, respectively. A web camera is installed to monitor the vegetation growth. A Raspberry Pi, an inexpensive embedded computer, is used to control the system and record the SNR data. The location of the vegetation sensor (40º01'52.15"N, 105º10'11.75"W) in Google Maps is shown in Fig. 5(b). The experiment period was from May 1, before the alfalfa sprouted, to August 13, after the alfalfa was harvested. The antennas are east oriented, and thus the south region, which has most ground tracks (each ground track is the footprint of the specular reflection points), is the optimal sensing area. Due to the distribution of the GPS satellites, there are few complete ground tracks to the north.

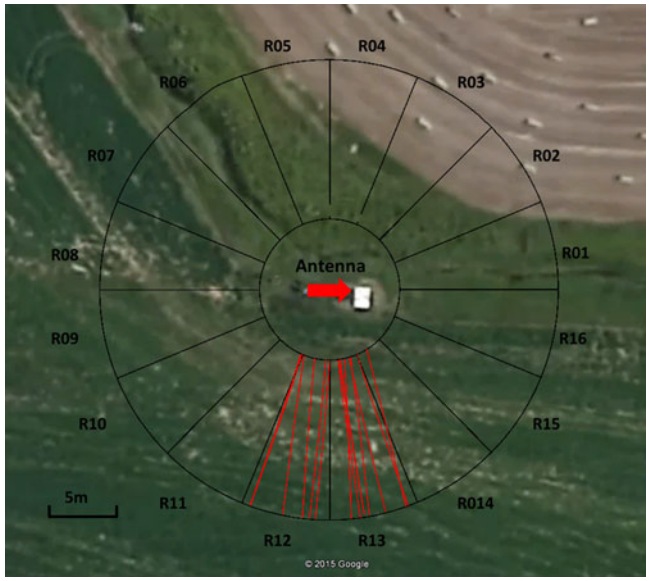

Fig. 6. Whole sensing region is evenly divided into 16 sectors. The two sectors in the south direction (R12 and R13) are the optimal sensing area because the antenna is east oriented. In the two sectors, there are about 12 ground tracks usable.

B. In Situ Data and GPS Data Collection

In situ measurements are needed to validate the GPS metric. During the experimental period, *in situ* data were sampled on a nearly weekly basis. In total, 11 field surveys were completed. The *in situ* vegetation measurements include vegetation height and VWC. For each vegetation sampling survey, seven 30-cm by 30-cm quadrats were selected randomly in the sensing region and their locations were recorded. Their distances from the antenna ranged from 7 to 34 m. The vegetation within each quadrat was clipped, weighed immediately (wet weight), dried in an oven at 50°C for 48 h, and weighed again (dry weight). The difference of the wet and dry weights represents the vegetation water mass, which is then normalized by the sampled area to obtain the VWC. The data from the seven sampled quadrats were averaged to get one day's *in situ* VWC measurement. Also, at each quadrat vegetation height was measured and then averaged

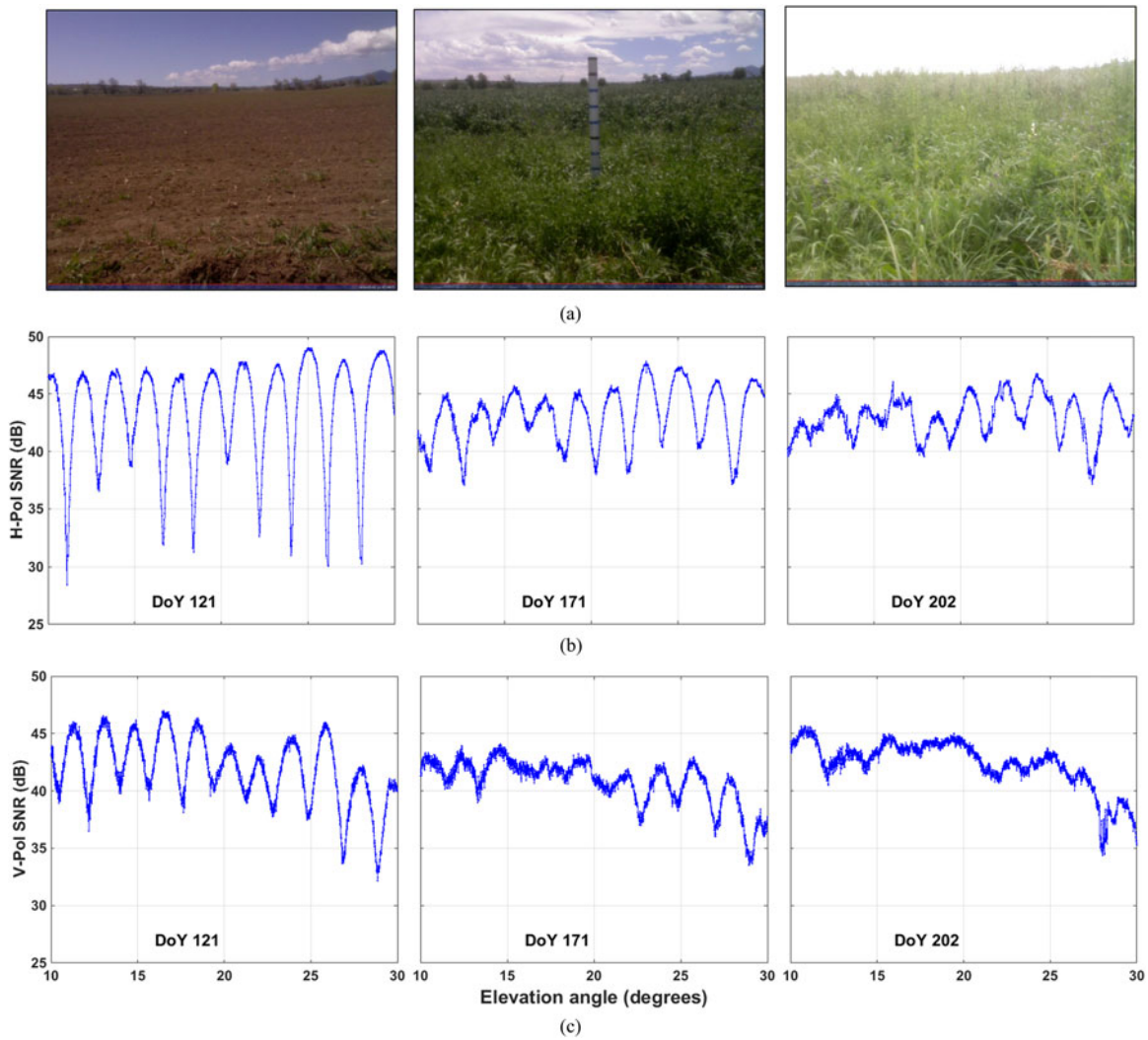

Fig. 7. (a) Photograph of field conditions, (b) H-pol SNR, and (c) V-pol SNR of PRN 13 in Region 13 on DoY 121, 171, and 202, 2014.

in the same way. Soil moisture data were sampled by Campbell Scientific 616 soil moisture probes at a rate of one sample per 30 min. The probes were distributed as follows: five probes were buried in soil at 2.5 cm, five were buried at 7.5 cm, and two were buried at 20 cm. Because the *L*-band sensing depth is ∼5 cm [30], we only utilize the 2.5-cm probe data here, which provide an average of the top 5 cm of the soil column. The 2.5-cm depth soil moisture data within one day were averaged to get a single day's soil moisture data representative of the top 5 cm of the soil column, as in [10].

The GlobalTop receivers output a customized NMEA message that includes the desired SNR information. The customized NMEA message can provide SNR resolved to 0.1 dB. Since a portion of commercial GPS receivers only provide quantized SNR resolved to 1 dB, we manually quantized the received SNR to 1 dB and found that the error introduced by quantization effect is negligible (less than 2%). The elevation angle mask used in the data processing is from 10° to 30°, resulting in the ground tracks extending from 5 to 20 m. There are approximately 70 GPS arcs (both rising and setting) that satisfy the elevation angle mask each day. The ground tracks are not evenly distributed in azimuth—most are in the southerly direction. The full azimuth direction is evenly divided into 16 sectors and the ground tracks in the two most south oriented sectors R12 and R13 are used to compute one day's SNR amplitude metric (see Fig. 6). For each ground track's SNR data, LSP is used to obtain the oscillation frequency of the interference pattern f_m (i.e., H_{eff}). As is shown later, the SNR data do not exhibit a rising trend as the geodetic SNR and thereby no detrending processing is required. Then, the amplitude is estimated using the least square method, with the oscillation frequency as the input. A quality check, using the ratio of postfit error to the amplitude as a goodness-of-fit indicator, is carried out to exclude the erroneous tracks. Finally, the estimated amplitudes that pass the quality check are averaged to be a single value, serving as the derived GPS metric for that particular day.

V. Experiment Results and Discussion

Three representative H-pol and V-pol SNR time series of PRN 13 that correspond to the beginning (DoY 121), middle

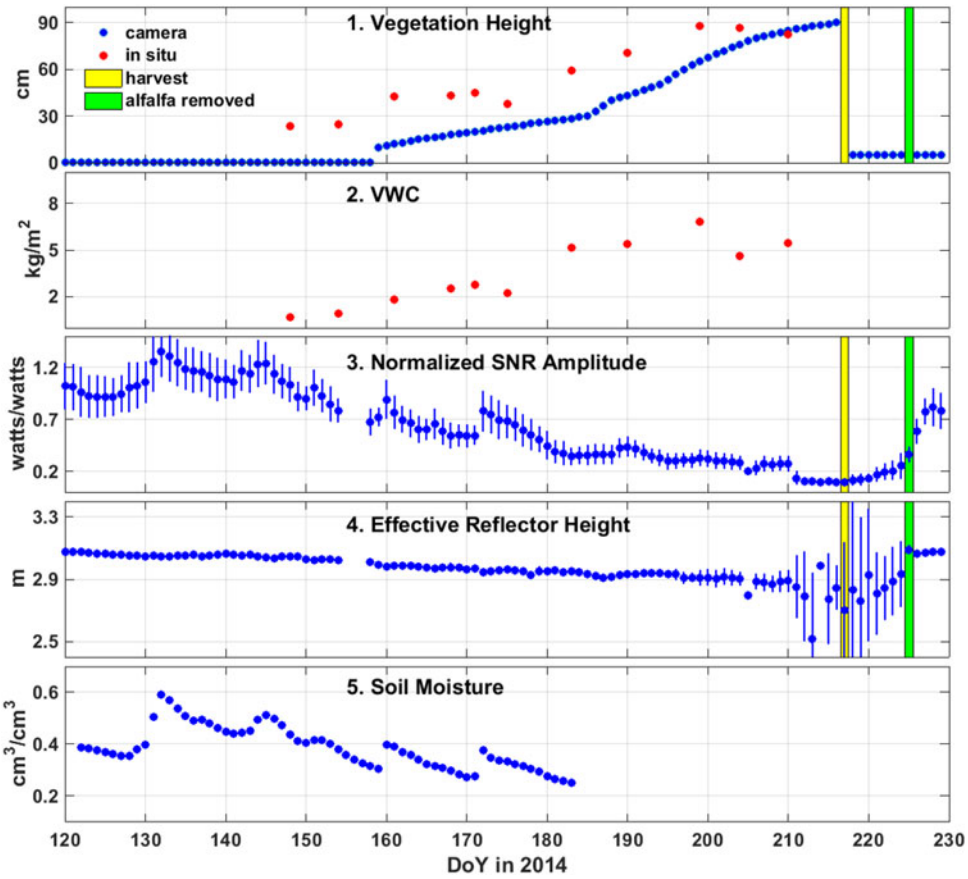

Fig. 8. Time series of (panel 1) vegetation height, (panel 2) VWC, (panel 3) normalized SNR amplitude A_{norm}, (panel 4) effective reflector height H_{eff}, and (panel 5) soil moisture from DoY 120 to 230. The error bars of panels 3 and 4 are based on the standard deviation of the measurements. Please note that the standard deviation of H_{eff} is only a few centimeter at the beginning of the vegetation growth (thus, the error bar is invisible), and then increases as vegetation grows. The vegetation is mowed on DoY 217, as is shown by the yellow bar. The cut vegetation was left in the field to dry, and then removed on DoY 225 (labeled by the green bar). The soil moisture data are not available after DoY 183 because of hardware issue.

(DoY 171), and end (DoY 202) phases of the vegetation growth cycle are presented in Fig. 7. In addition, photographs of the corresponding days are included to show the field conditions. The azimuth angle of PRN 13 during the observation time is $\sim$175°, locating in the optimal sensing area of the horizontal antenna. The V-pol antenna is omnidirectional and, thus, has no preference as to the azimuth direction. Before the alfalfa sprouted (DoY 121), both the H-pol and V-pol SNR show a distinct interference pattern. The interference pattern of the H-pol SNR has deeper nulls than the V-pol SNR, indicating that more reflection power is absorbed by the horizontal antenna. This matches the simulation results – $|R_h|$ is greater than $|R_v|$ for bare soil case. The interference pattern of the V-pol SNR has a notch in amplitude when elevation angle is around 22°. This should be attributed to the Brewster's angle of the V-pol reflection. The V-pol interference pattern does not completely diminish at the Brewster's angle, perhaps because of the nonuniformity of the surface soil layer as well as the surface roughness. Using the *in situ* soil moisture data and the soil permittivity–moisture model in [31], we obtain a theoretical Brewster's angle of 24°, which is close to what is observed in V-pol SNR data. There are also some mismatches between experimental data and simulation results. For example, simulated V-pol SNR at low-elevation angles (below 13°) shows irrelevance to vegetation growth while the experimental V-pol SNR data show a uniformly decreasing trend even at low elevation angles. This discrepancy indicates the limitations of the layered model—the inhomogeneities of the vegetation layer and the inside volume scattering are not incorporated. Also for this reason, we use a relatively large cutoff elevation angle (10°) because an obvious drop in SNR amplitude is observed when elevation angles are below 10°.

As the vegetation grows, we can see a drop in the H-pol SNR amplitude, which also matches the simulation results in Section III. For the V-pol SNR, the interference patterns are blurred as the vegetation grows. It is difficult to identify any notch in the V-pol SNR data from DoY 171 and 202. In contrast, notches were observed in [12], [26] and [27] throughout the experimental cycle. The results presented here and those from [12], [26], [27] are not expected to be the same: the primary reason is that different antennas (patch versus dipole) were used in the two experiments; also, different types of vegetation (wheat, barley, maize versus alfalfa) were studied.

The time series of vegetation height (both *in situ* and camera), *in situ* VWC, normalized SNR amplitude A_{norm}, effective reflector height H_{eff}, and soil moisture from the observation period are presented in Fig. 8. The vegetation was cut on DoY

217 (labeled by the yellow bar), then removed from the field on DoY 225 (labeled by the green bar). The raw SNR amplitude time series are normalized by the average of amplitude measurements from DoY 120 to 123. During these four days, the vegetation had not yet sprouted. In addition, there were no precipitation events so the soil moisture was relatively constant. In the following interval, precipitation increases the soil moisture and, thus, the reflection power. As a result, the normalized SNR amplitude is greater than 1 on some days.

The normalized SNR amplitude $A_{\rm norm}$ clearly decreases as the vegetation grows (see Fig. 8, panels 1, 2, and 3), from the value of 1.0 at the start of the observation period to close to zero prior to the alfalfa cutting. During this interval, vegetation height increases from 0 to 90 cm and VWC increases from 0 to 6 kg/m^2. The high amplitude values between days 130 and 150 show the effect of increasing soil moisture, prior to the sprouting of the alfalfa. Once the alfalfa sprouts, there is a nearly monotonic decrease in $A_{\rm norm}$ as vegetation height and VWC increase. This decrease occurs over a range of VWC of 0—6 kg/m^2. Importantly, $A_{\rm norm}$ does not increase after the vegetation harvest on DoY 217, which indicates that $A_{\rm norm}$ is not sensitive to vegetation height. In contrast, $A_{\rm norm}$ does increase dramatically (almost to 1.0) once the cut vegetation is removed from the field on DoY 225. This shows that $A_{\rm norm}$ is affected directly by the variations in VWC. The apparent relationship between $A_{\rm norm}$ and vegetation height is the outcome of a linear correlation between vegetation height and VWC during the growth period. Panels 3 and 5 show that the general decline in $A_{\rm norm}$ is temporarily affected by abrupt increases in soil moisture due to precipitation or irrigation. These sharp increases in soil moisture increase the permittivity of soil and the H-pol reflection coefficient, as shown in Fig. 3.

It is demonstrated that the effective reflector height $H_{\rm eff}$ derived from geodetic SNR is not a reliable indicator of vegetation change [23]. From panel 4 of Fig. 8, $H_{\rm eff}$ linearly decreases from $\sim$3.1 m (bare soil) at the beginning to $\sim$2.8 m prior to harvest ($\sim$1 m vegetation). The decrease of $H_{\rm eff}$ is much smaller than the increase of vegetation canopy height (0.3 m versus 1 m), indicating that the soil surface is still the primary reflector even with high vegetation. Moreover, $H_{\rm eff}$ becomes unreliable when the vegetation height reaches a particular threshold prior to the harvest: the average $H_{\rm eff}$ behaves randomly and the standard deviation greatly increases. The reason for the randomized $H_{\rm eff}$ and the increased errors is likely the high-vegetation LSP has two peaks and the maximum peak alternates, as demonstrated in [23].

Fig. 9 shows that a clear negative correlation exists between $A_{\rm norm}$ and the *in situ* measurements of VWC. The uncertainties shown are based on the standard deviation of the $A_{\rm norm}$ observations and *in situ* measurements. The R^2 is 0.82, indicating a good agreement between the two variables. From the model, which has been fit to the data, the sensitivity of $A_{\rm norm}$ to VWC is -0.11 (W/W)/(kg/m^2). The maximum *in situ* VWC exceeds 6 kg/m^2, which is much greater than the maximum VWC detectable using geodetic GPS data ($\sim$1.0 kg/m^2). The average measurement error of VWC using $A_{\rm norm}$ and the fit linear model is 12.4%. Fig. 10 shows the correlation between $A_{\rm norm}$ and the

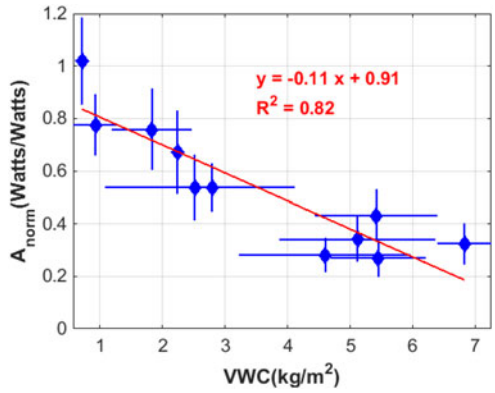

Fig. 9. Correlation between $A_{\mathbf{norm}}$ and VWC. Both the $A_{\mathbf{norm}}$ and *in situ* VWC uncertainties are based on the observation standard deviation. The regression yields $A_{\mathbf{norm}} = -0.11 * \mathbf{VWC} + 0.91$ with a $R^2 = 0.82$. The 95% confidence level of slope coefficient is -0.11 ± 0.03.

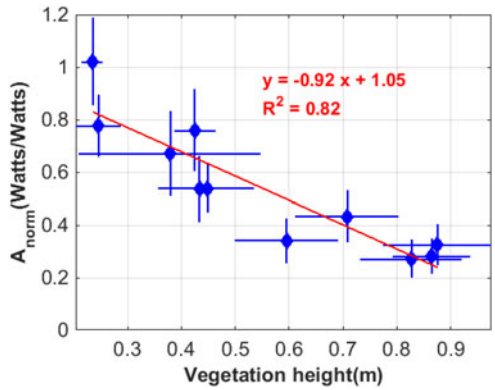

Fig. 10. Correlation between $A_{\mathbf{norm}}$ and vegetation height. Both the $A_{\mathbf{norm}}$ and *in situ* vegetation height uncertainties are based on the observation standard deviation. The regression yields $A_{\mathbf{norm}} = -0.92 * \mathbf{VH} + 1.05$ with a $R^2 = 0.82$. The 95% confidence level of slope coefficient is -0.92 ± 0.32.

in situ vegetation height is similarly high ($R^2 = 0.82$). Generalizing the results, we can say the normalized SNR amplitude $A_{\rm norm}$ shows a linear relationship with the *in situ* measurements of the vegetation biophysical parameters (VWC and vegetation height). The simulation results in [23] show that $A_{\rm norm}$ derived from geodetic SNR is linearly decreasing as VWC increases provided that VWC is below 1.5 kg/m^2, and then saturates. Because the GPS antenna and vegetation type in this experiment are different, we resimulate the responses of $A_{\rm norm}$ with vegetation growth, as shown in Fig. 11. We can see that the magnitude of the simulated decreasing slope is close to but smaller than that fit by actual data. This discrepancy should be attributed to the unmodeled inhomogeneities and volume scattering of the vegetation canopy, which would bring in additional signal power loss.

From Fig. 8 $A_{\rm norm}$ is clearly affected by the change of soil moisture as well as the vegetation growth. Here, we make use of the multiple precipitation events to evaluate the soil moisture effect on $A_{\rm norm}$. Before the alfalfa sprouts, the soil roughness is quite stable and the change of $A_{\rm norm}$ should be attributed to the change of the soil moisture. With the *in situ* soil moisture data, we can simulate the change of $A_{\rm norm}$ using the soil permittivity–moisture model in [31] and the $A_{\rm norm}$-ε_r model presented in

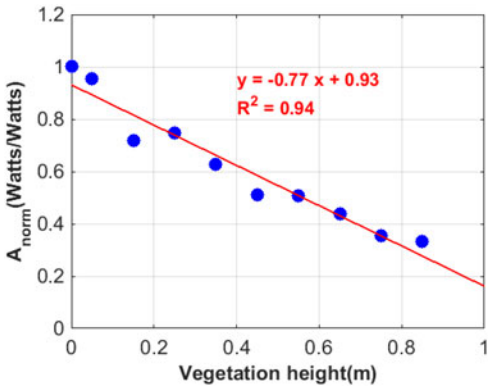

Fig. 11. Simulated $A_{\rm norm}$ versus vegetation height. The vegetation permittivity used in the simulation is $1.06 + 0.015$j, which is derived from *in situ* vegetation measurements.

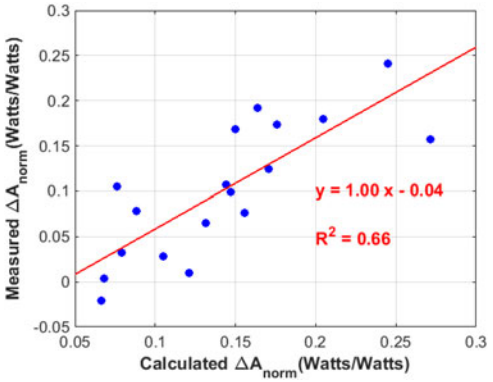

Fig. 12. Measured $A_{\rm norm}$ change versus calculated $A_{\rm norm}$ change from *in situ* soil moisture data before alfalfa sprouts. With soil moisture, soil permittivity is calculated using the model presented in [31] and the $A_{\rm norm}$ change is calculated using the model presented in [23].

[23]. The relationship of the simulated and actual $A_{\rm norm}$ change ($\Delta A_{\rm norm}$) is shown in Fig. 12 and the regression has a slope of 1.00 and R^2 of 0.66, which validates the effectiveness of the model used in the simulation of bare soil. Based on this calculation, the change of $A_{\rm norm}$ introduced by precipitation or irrigation is estimated to be no larger than 24% during the experiment period.

VI. Conclusion

In this paper, we analyzed the requirement of vegetation growth sensing using GPS-IR and selected/utilized horizontal polarization for a vegetation sensing experiment. A customized horizontally polarized dipole antenna is proposed and evaluated in an experiment carried out at Boulder, CO, USA. Both modeled and experimental data show that the soil surface is the primary reflector even with dense-water vegetation. The experiment results show that there is a negative, linear relationship between the normalized SNR amplitude and VWC over a range of 0—6 kg/m^2. The sensitivity of $A_{\rm norm}$ to VWC change is -0.11 (W/W)/(kg/m^2), and the average measurement error of VWC is 12.4%. This measurement range is much greater than that detectable using standard geodetic systems or a vertically polarized dipole antenna. The extended measurement range is due to the increased reception capability of the dipole antenna used in the experiment. The effect of the soil moisture change is also observed, and produces relatively smaller changes in normalized SNR amplitude.

References

[1] C. J. Tucker, J. E. Pinzon, M. E. Brown, D. A. Slayback, E. W. Pak, R. Mahoney *et al.*, "An extended AVHRR 8-km NDVI dataset compatible with MODIS and SPOT vegetation NDVI data," *Int. J. Remote Sens.*, vol. 26, pp. 4485–4498, 2005.

[2] M. Owe, R. de Jeu, and J. Walker, "A methodology for surface soil moisture and vegetation optical depth retrieval using the microwave polarization difference index," *IEEE Trans. Geosci. Remote Sens.*, vol. 39, no. 8, pp. 1643–1654, Aug. 2001.

[3] K. M. Larson, E. D. Gutmann, V. U. Zavorotny, J. J. Braun, M. W. Williams, and F. G. Nievinski, "Can we measure snow depth with GPS receivers?" *Geophysical Res. Lett.*, vol. 36, no. 17, 2009.

[4] F. G. Nievinski and K. M. Larson, "Inverse modeling of GPS multipath for snow depth estimation—Part I: Formulation and simulations," *IEEE Trans. Geosci. Remote Sens.*, vol. 52, no. 10, pp. 6555–6563, Oct. 2014.

[5] F. G. Nievinski and K. M. Larson, "Inverse modeling of GPS multipath for snow depth estimation—Part II: Application and validation," *IEEE Trans. Geosci. Remote Sens.*, vol. 52, no. 10, pp. 6564–6573, Oct. 2014.

[6] N. Rodriguez-Alvarez *et al.*, "Snow thickness monitoring using GNSS measurements," *IEEE Geosci. Remote Sens. Lett.*, vol. 9, no. 6, pp. 1109–1113, Nov. 2012.

[7] K. Boniface, J. J. Braun, J. L. McCreight, and F. G. Nievinski, "Comparison of snow data assimilation system with GPS reflectometry snow depth in the Western United States," *Hydrological Processes*, vol. 29, pp. 2425–2437, 2015.

[8] S. G. Jin and N. Najibi, "Sensing snow height and surface temperature variations in Greenland from GPS reflected signals," *Adv. Space Res.*, vol. 53, pp. 1623–1633, Jun. 1 2014.

[9] K. M. Larson *et al.*, "GPS multipath and its relation to near-surface soil moisture content," *IEEE J. Sel. Topics Appl. Earth Observations Remote Sens.*, vol. 3, no. 1, pp. 91–99, Mar. 2010.

[10] K. M. Larson, E. E. Small, E. D. Gutmann, A. L. Bilich, J. J. Braun, and V. U. Zavorotny, "Use of GPS receivers as a soil moisture ne twork for water cycle studies," *Geophysical Res. Lett.*, vol. 35, 2008.

[11] V. U. Zavorotny *et al.*, "A physical model for gps multipath caused by land reflections: Toward bare soil moisture retrievals," *IEEE J. Sel. Topics Appl. Earth Observations Remote Sens.*, vol. 3, no. 1, pp. 100–110, Mar. 2010.

[12] N. Rodriguez-Alvarez *et al.*, "Land geophysical parameters retrieval using the interference pattern GNSS-R technique," *IEEE Trans. Geosci. Remote Sens.*, vol. 49, no. 1, pp. 71–84, Jan. 2011.

[13] A. Alonso-Arroyo *et al.*, "Improving the accuracy of soil moisture retrievals using the phase difference of the dual-polarization GNSS-R interference patterns," *IEEE Geosci. Remote Sens. Lett.*, vol. 11, no. 12, pp. 2090–2094, Dec. 2014.

[14] A. A. Arroyo *et al.*, "Dual-polarization GNSS-R interference pattern technique for soil moisture mapping," *IEEE J. Sel. Topics Appl. Earth Observations Remote Sens.*, vol. 7, no. 5, pp. 1533–1544, May 2014.

[15] K. M. Larson, J. S. Lofgren, and R. Haas, "Coastal sea level measurements using a single geodetic GPS receiver," *Adv. Space Res.*, vol. 51, pp. 1301–1310, 2013.

[16] J. S. Lofgren, R. Haas, and J. M. Johansson, "Monitoring coastal sea level using reflected GNSS signals," *Adv. Space Res.*, vol. 47, pp. 213–220, 2011.

[17] J. S. Lofgren, R. Haas, H. G. Scherneck, and M. S. Bos, "Three months of local sea level derived from reflected GNSS signals," *Radio Sci.*, vol. 46, 2011.

[18] A. Alonso-Arroyo *et al.*, "Retrieval of significant wave height and mean sea surface level using the GNSS-R interference pattern technique: Results from a three-month field campaign," *IEEE Trans. Geosci. Remote Sens.*, vol. 53, no. 6, pp. 3198–3209, Jun. 2015.

[19] E. E. Small, K. M. Larson, and J. J. Braun, "Sensing vegetation growth with reflected GPS signals," *Geophysical Res. Lett.*, vol. 37, 2010.

[20] K. M. Larson and E. E. Small, "Normalized microwave reflection index: A vegetation measurement derived from GPS networks," *IEEE J. Sel. Topics Appl. Earth Observations Remote Sens.*, vol. 7, no. 5, pp. 1501–1511, May 2014.
[21] E. E. Small, K. M. Larson, and W. K. Smith, "Normalized Microwave Reflection Index: Validation of Vegetation Water Content Estimates From Montana Grasslands," *IEEE J. Sel. Topics Appl. Earth Observations Remote Sens.*, vol. 7, no. 5, pp. 1512–1521, May 2014.
[22] W. Wan, K. M. Larson, E. E. Small, C. C. Chew, and J. J. Braun, "Using geodetic GPS receivers to measure vegetation water content," *GPS Solutions*, vol. 19, pp. 237–248, Apr. 2015.
[23] C. C. Chew, E. E. Small, K. M. Larson, and V. U. Zavorotny, "Vegetation sensing using GPS-interferometric reflectometry: Theoretical effects of canopy parameters on signal-to-noise ratio data," *IEEE Trans. Geosci. Remote Sens.*, vol. 53, no. 5, pp. 2755–2764, May 2015.
[24] K. M. Larson and E. E. Small, "Using GPS to study the terrestrial water cycle," *Eos, Trans. Amer. Geophysical Union*, vol. 94, pp. 505–506, 2013.
[25] Q. Chen, D. Won, and D. M. Akos, "Sno w depth sensing using the GPS L2C signal with a dipole antenna," *Eurasip J. Adv. Signal Process.*, no. 2014, 2014.
[26] N. Rodriguez-Alvarez, X. Bosch-Lluis, A. Camps, A. Aguasca, M. Vall-Ilossera, and E. Valencia *et al.*, "Review of crop growth and soil moisture monitoring from a ground-based instrument implementing the Interference Pattern GNSS-R Technique," *Radio Sci.*, vol. 46, 2011.
[27] N. Rodriguez-Alvarez *et al.*, "Soil moisture retrieval using GNSS-R techniques: Experimental results over a bare soil field," *IEEE Trans. Geosci. Remote Sens.*, vol. 47, no. 11, pp. 3616–3624, Nov. 2009.
[28] F. G. Nievinski and K. M. Larson, "Forward modeling of GPS multipath for near-surface reflectometry and positioning applications," *GPS Solutions*, vol. 18, pp. 309–322, Apr. 2014.
[29] F. T. Ulaby and E. A. Wilson, "Microwave attenuation properties of vegetation canopies," *IEEE Trans. Geosci. Remote Sens.*, vol. GE-23, no. 5, pp. 746–753, Sep. 1985.
[30] T. J. Jackson *et al.*, "Validation of soil moisture and ocean salinity (SMOS) soil moisture over watershed networks in the U.S.," *IEEE Trans. Geosci. Remote Sens.*, vol. 50, pp. 1530–1543, May 2012.
[31] M. T. Hallikainen *et al.*, "Microwave dielectric behavior of wet soil. 1. Empirical–Models and Experimental-Observations," *IEEE Trans. Geosci. Remote Sens.*, vol. GRS-23, no. 1, pp. 25–34, Jan. 1985.

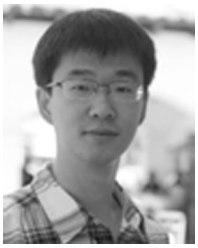

Qiang Chen received the Ph.D. degree in aerospace engineering sciences from the University of Colorado at Boulder, CO, USA, in 2016. His research focuses on instrument optimization for GPS Interferometric Reflectometry remote sensing.

Daehee Won received his Ph.D. degree in aerospace information engineering from the Konkuk University, Seoul, South Korea, in 2013. He is a Research Associate of aerospace engineering sciences at the University of Colorado at Boulder, CO, USA. His research interests include GNSS precise positioning, sensor integration, and GPS-IR remote sensing.

Dennis M. Akos received his Ph.D. degree in electrical and computer engineering from the Ohio University, Athens, OH, USA, in 1997. He is a Professor of aerospace engineering sciences at the University of Colorado at Boulder. His research interests include GNSS, software-defined radio, digital signal processing, and radio-frequency design.

Eric E. Small received his Ph.D. degree in earth sciences from the University of California at Santa Cruz, CA, USA, in 1998. He is a Professor of geological sciences at the University of Colorado at Boulder, CO, USA. His current research focuses on land surface hydrology.